Landau pole induced vorticity growth in a class of non-monotonic shear flows

2008 J. Phys. A: Math. Theor. 41 145501

(http://iopscience.iop.org/1751-8121/41/14/145501)

IOP PUBLISHING JOURNAL OF PHYSICS A: MATHEMATICAL AND THEORETICAL

J. Phys. A: Math. Theor. **41** (2008) 145501 (17pp) doi:10.1088/1751-8113/41/14/145501

Landau pole induced vorticity growth in a class of non-monotonic shear flows

Francesco Volponi[1] **and Marco Okolicsanyi**[2]

[1] Cannaregio 4781, 30121 Venezia, Italy
[2] Via Genova 8, 35142 Padova, Italy

E-mail: foxonif@yahoo.co.jp and mokolic@virgilio.it

Received 12 November 2007, in final form 12 February 2008
Published 26 March 2008
Online at stacks.iop.org/JPhysA/41/145501

Abstract

A vorticity growth mechanism leading to the creation of two-dimensional inviscid vortices is presented. The vorticity amplification saturates to values two orders of magnitude larger than those of the initial disturbance. The growth occurs because of a resonance with a Landau pole of the system and strongly depends on the value of the initial perturbation at the point of inflection of the equilibrium profile. These findings are obtained by numerically solving the initial-value problem associated with the Rayleigh equation. Numerical solution of the corresponding eigenvalue problem and direct numerical computation of the Landau pole give consistent results.

PACS numbers: 47.15.Fe, 47.15.ki, 47.20.Ft, 47.32.C

1. Introduction

Many flows occurring in fluid systems can be treated as two dimensional [1–3]. These flows often organize in one or more vortices. One thoroughly studied example is represented by the inviscid decay of asymmetries on a stable circular vortex [1, 4, 5]. In [1] this phenomenon was studied both experimentally and theoretically by comparing data relative to magnetized electron plasmas in a cylindrical Penning trap with results based on the analysis of the linearized 2D Euler equations. It was shown that the initial stage of exponential decay of asymmetries in experiments is governed by linear theory, while over longer times nonlinear effects emerge.

The linear decay rate is given by the imaginary part of a so-called Landau pole. A Landau pole is a complex frequency c_L at which the temporal Laplace transform of the streamfunction becomes singular [4, 6]: its value depends only on the equilibrium velocity profile and not on the initial perturbation. In [1] it was shown as well that, while the disturbance streamfunction decays exponentially in the initial phase, a vorticity perturbation grows in the neighbourhood of a critical radius r_c dependent on the frequency $\mathrm{Re}(c_L)$ of the Landau pole. Eventually, the vorticity bump growth saturates to values comprised between 10^{-2} and 10^{-1} of the initial

vorticity perturbation peak. This saturated growth mechanism will be important for the present study.

Other natural systems whose dynamics seems to be ruled by approximately 2D inviscid flows are given by the atmospheres of outer planets. These atmospheres are characterized by zonal winds, traditionally seen as confined to a thin layer near the cloud tops, and dominated by large vortical structures such as the Great Red Spot in Jupiter. In this planet and Saturn zonal winds strongly vary with latitude and have a marked non-monotonic dependence on it with multiple maxima and minima [3]. Our goal in the present study is to investigate the effect of non-monotonicity of flow profiles on the evolution of disturbances.

Mathematically, inviscid flows are described by the Euler equations. Their evolution in a linear regime is described by the Rayleigh equation, which constitutes the starting point of the stability analysis of shear flows. Before introducing our main results we briefly summarize main facts about the mathematical structure of the Rayleigh equation.

The eigenspectrum of the Rayleigh equation has a discrete and a continuous component. The first is governed by the Rayleigh inflection point theorem [7]—a necessary condition for instability is the presence of an inflection point in the velocity profile. An important generalization of this theorem was due to Fjørtoft [8], who restricted the class of possibly unstable flows. The continuous branch was shown to be stable [9–11] for monotonic flow profiles. A rigorous treatment discussing the contribution of the continuous spectrum in the presence of non-monotonic profiles has never been given.

Smith and Rosenbluth [2] showed, however, that in a setting similar to the Rayleigh equation, 2D inviscid vorticity equation in a cylindrical geometry, and for angular velocity profiles with a stationary point, the azimuthal wave number $m = 1$ mode grows algebraically as the square root of time. The origin of this instability, associated with the continuous spectrum of the evolution operator, stays in phase coherence.

The Rayleigh equation has been thoroughly studied for monotonic flow profiles; in that context, unstable solutions have a global character and a clear exponential evolution.

In this paper, it will be shown how a departure from the monotonic assumption can lead to modifications of the classical paradigm. We will present a solution of the initial-value problem associated with the Rayleigh equation relative to a non-monotonic velocity equilibrium profile of the type $f(y) = a + y^3 - by$ (a and b are positive, real parameters) directed along the x-axis in a channel $[-1, 1]$. The vorticity evolution is characterized by a localized and slow growth which eventually saturates to values of order 10^2 with respect to the initial vorticity perturbation peak, in contrast with the common understanding of traditional inflectional instabilities. The localized growth occurs at points where the perturbation vorticity oscillates in resonance with the value of the flow at the inflection point, y_s. Moreover, it strongly depends on the initial value of the perturbation at y_s—the vanishing of the initial disturbance at y_s suppresses the growth.

We chose the class of profiles $f(y) = a + y^3 - by$ because it represents the simplest non-monotonic flow endowed with a maximum and a minimum. We preferred a polynomial equilibrium with respect to sinusoidal flows of the type $\sin \beta y$ (where β is a real number) for two reasons. The first is given by the fact that sinusoidal profiles have been studied and shown to lead to violent global exponential instabilities of the Kelvin–Helmholtz type, while we found that the polynomial profile under study, in spite of the fact that satisfies the Rayleigh–Fjørtoft necessary condition for instability, it is not subject to fast exponential instabilities for any value of the wave number k for $b < 0.85$ (for $b > 0.85$ global exponential growth occurs for appropriate values of k). The second is that, in the polynomial profile, points y_p for which holds the relation $f(y_p) = f(y_s)$ are not inflection points themselves as it occurs in sinusoidal profiles, a condition which appears too restrictive.

We observed as well that, analogously to the findings in [1], the growth of vorticity in the resonant layer is accompanied by the global exponential decay of the disturbance streamfunction. This brings us to conclude that the mechanism underlying the saturated growth of vorticity is essentially the same found in [1], but much stronger. Mathematically, a Landau pole of frequency $\mathrm{Re}(c_L)$ causes growth of an initial vorticity perturbation with expansion coefficients, calculated with respect to the eigenfunctions of the system, peaked around $\mathrm{Re}(c_L)$.

2. Initial-value problem

Let us consider an inviscid incompressible fluid. This system is described by Euler equations

$$\nabla \cdot \mathbf{V} = 0, \tag{1}$$

$$\partial_t \mathbf{V} + \mathbf{V} \cdot \nabla \mathbf{V} = -\nabla P, \tag{2}$$

where $\mathbf{V}$ and P are the velocity and pressure fields respectively. By taking the curl of equation (2) we obtain the vorticity equation

$$\partial_t \mathbf{\Omega} - \nabla \times (\mathbf{V} \times \mathbf{\Omega}) = 0, \tag{3}$$

where $\mathbf{\Omega} = \nabla \times \mathbf{V}$ is the vorticity. Considering two-dimensional flows and assuming a symmetry with respect to the z component, we can express the velocity field in terms of the stream function Φ as

$$\mathbf{V} = \nabla \Phi \times \mathbf{e}_z, \tag{4}$$

where $\mathbf{e}_z$ is a unit vector normal to the plane of the flow. The vorticity is parallel to $\mathbf{e}_z$ and is related to the stream function via the Poisson equation $\Omega = -\Delta\Phi$ (Δ is the Laplacian). Substituting (4) into (3) gives

$$\partial_t \Omega + \mathbf{V} \cdot \nabla \Omega = 0. \tag{5}$$

By decomposing stream function, velocity and vorticity fields as

$$\Phi = \Phi_0 + \phi, \qquad \mathbf{V} = \mathbf{V}_0 + \mathbf{v}, \qquad \Omega = \Omega_0 + \omega, \tag{6}$$

where $\Phi_0, \mathbf{V}_0$ and Ω_0 represent the equilibrium and ϕ, $\mathbf{v}$ and ω the perturbation fields, equation (5) can be linearized to give

$$\partial_t \omega + \mathbf{V}_0 \cdot \nabla \omega + \mathbf{v} \cdot \nabla \Omega_0 = 0. \tag{7}$$

Assuming a parallel equilibrium flow of the form $\mathbf{V}_0 = (-f(y), 0, 0)$, equation (7) becomes

$$(\partial_t - f(y)\partial_x)\Delta\phi = -f''(y)\partial_x\phi, \tag{8}$$

where $' = \partial_y$. Since the ambient field is homogeneous with respect to x, we can decompose ϕ into Fourier modes proportional to $\mathrm{e}^{\mathrm{i}kx}$. Writing $\partial_x = \mathrm{i}k$ with a good quantum number k (in what follows $k > 0$) the Laplacian becomes $\Delta = \partial_y^2 - k^2$ and equation (8) translates as

$$[\partial_t - \mathrm{i}kf(y)]\Delta\phi = -\mathrm{i}kf''(y)\phi, \tag{9}$$

which is the celebrated Rayleigh equation with boundary conditions $\phi(-1) = \phi(+1) = 0$.

By inverting the Laplacian operator Δ in $[-1, 1]$, with ϕ vanishing at the boundary, we can express the stream function in terms of the vorticity [12] with

$$\phi = -\Delta^{-1}\omega = -\int_{-1}^{1} G(y, \bar{y})\omega(\bar{y}, t)\,\mathrm{d}\bar{y}, \tag{10}$$

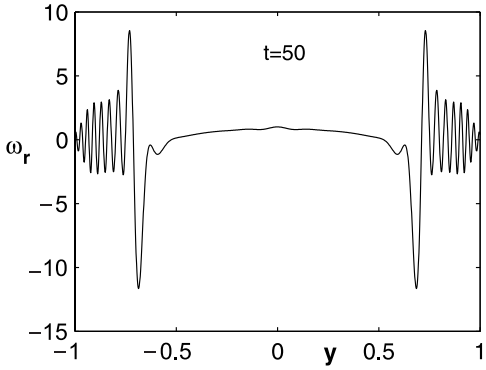

Figure 1. Real part of the disturbance at $t = 50$ for $f(y) = y^3 - 0.49y$ and $\omega(y, 0) = \cos(y)$.

where

$$G(y, \bar{y}) = -\begin{cases} \dfrac{\sinh[k(1+y)]\sinh[k(1-\bar{y})]}{k\sinh(2k)} & (-1 \leqslant y \leqslant \bar{y}) \\ \dfrac{\sinh[k(1-y)]\sinh[k(1+\bar{y})]}{k\sinh(2k)} & (\bar{y} \leqslant y \leqslant 1). \end{cases} \tag{11}$$

By substituting (10) into (9) we have

$$[\partial_t - \mathrm{i}kf(y)]\omega = -\mathrm{i}kf''(y)\int_{-1}^{1} G(y, \bar{y})\omega(\bar{y}, t)\,\mathrm{d}\bar{y}. \tag{12}$$

We investigated the stability of the above equation for the class of non-monotonic profiles $f(y) = a + y^3 - by$ (a and b are positive, real parameters). Numerical time integration of equation (12) has been carried out by means of a second-order Runge–Kutta routine, while the spatial integral on the right-hand side of (12) has been computed by Simpson integration evaluating the integrand at N points (for the present simulations $N = 2001$).

The numerical solution breaks down after a time $\tau \sim \frac{2\pi}{C}$, where $C = \max_{y\in[-1,1]} |kf'(y)\Delta y|$ ($\Delta y = \frac{2}{N-1}$ is the grid-point spacing). This happens because, for $t > \tau$, the variation of ω in y becomes so fast that the numerical estimate of the integral on the right-hand side of equation (12) diverges from the exact value.

The integration scheme has been tested for various profiles ($\sin \beta y$, Poiseuille and others) and has led to results in complete agreement with the existing literature. Moreover, the results of the numerical integration were found to be independent on the spatial and temporal discretizations. Spatially, results obtained for $N = 1001, 2001$ and 4001 are identical. Temporally, increasing the time resolution by a factor 10 did not lead to any modification of the results. We as well checked our program by upgrading the second-order Runge–Kutta routine to a fourth-order Runge–Kutta and by changing Simpson with Gauss integration for the computation of the space integral in (12). No appreciable changes were found.

In this section, we will present the results obtained for $a = 0$ and $b = 0.49$ (i.e. the profile $f(y) = y^3 - 0.49y$), while their interpretation will be given in the following section by means of eigenspectrum analysis. Similar results are obtained for different values of a and b. In all simulations below we consider for the wave number the value $k = 2$, since around this value fast growth of disturbances was noted.

Initial conditions have a very strong effect on the observed growth. We consider first the initial perturbation $\omega(y, 0) = \cos(y)$. After an initial phase where the position y_p of the peaks of the solution varies (figures 1 and 2), at times $t \sim 300$, y_p tunes around the values ± 0.7 and

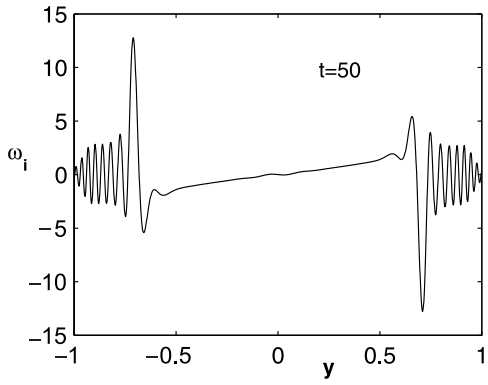

Figure 2. Imaginary part of the disturbance at $t = 50$ for $f(y) = y^3 - 0.49y$ and $\omega(y, 0) = \cos(y)$.

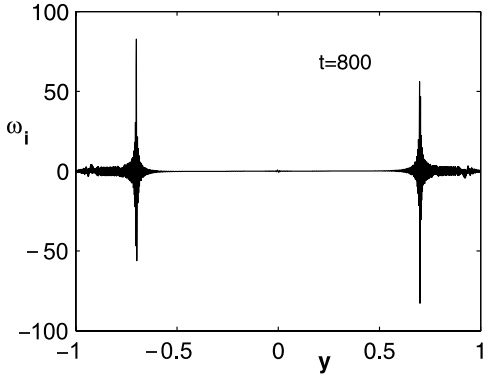

Figure 3. Imaginary part of the disturbance at $t = 800$ for $f(y) = y^3 - 0.49y$ and $\omega(y, 0) = \cos(y)$.

there it stays (figures 3 and 4). To be precise, the imaginary part of the solution ω_i has maxima at ± 0.7 and the real part ω_r has it at ± 0.699. We have noted that for any value of N, ω_r has maxima at the points $\pm(0.7 - 2/(N - 1))$. This suggests that the tiny discrepancy between the position of the peaks for ω_i and ω_r is a result of the discretization procedure implicit in the numerical solution and that, therefore, in the continuum limit the peaks of ω_r occur as well at ± 0.7. The position y_p of the peaks is an important aspect of the present growth because it suggests their resonance with the point $y_s = 0$, where the profile $f(y)$ possesses an inflection point ($f''(y_s) = 0$); in fact in y_p we have $f(y_p) = f(y_s)$. This is confirmed by simulations carried out for different values of a and b. The growth is localized in a neighbourhood of y_p, while outside this region only oscillations pertain. The growth is slow and saturates for $t \to \infty$ to values ~ 90. In figure 5 we present the time evolution of ω_i at the resonant point y_p. The graph suggests that in the solution there is no phase dependence of the type $e^{ikf(y)t}$. This is understandable if we consider that $f(y_p) = 0$. To check this fact we carried out simulations for the profile $f(y) = 1 + y^3 - 0.49y$. The results confirm the above-exposed behaviour with the addition of a phase dependence of the type $e^{ikf(y_p)t}$ at y_p.

The characterizing features of the present growth are quite distant from the usual picture regarding inflectional instabilities, which arise in the context of the Rayleigh equation. Slow growth and creation of localized structures counterpose to fast exponential time divergence and globally evolving solutions.

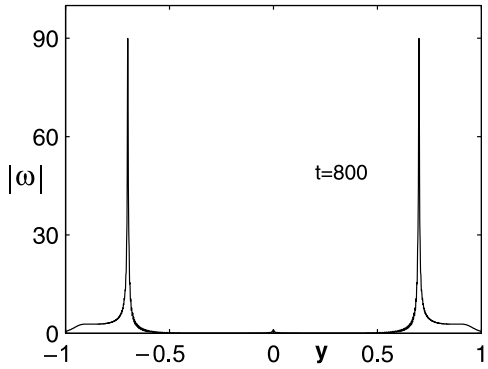

Figure 4. Absolute value of the disturbance vorticity at $t = 800$ for $f(y) = y^3 - 0.49y$ and $\omega(y, 0) = \cos(y)$.

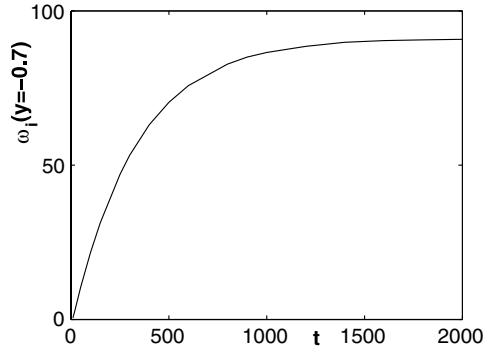

Figure 5. Evolution of the imaginary part of the disturbance vorticity at $y = -0.7$ for $f(y) = y^3 - 0.49y$ and $\omega(y, 0) = \cos(y)$.

Another peculiar feature of the present solution is represented by its critical dependence on the initial condition. Precisely, the growth is affected by the value of the initial perturbation at the inflection point. We carried out simulations relative to many initial conditions satisfying $\omega(y_s, 0) = 0$, all leading to the same type of behaviour. In figure 6 we present the case $\omega(y, 0) = \sin(y)$. It is evident that the growth is essentially suppressed. For $t = 800$ a growing structure is still present at y_p, but its size is drastically reduced in comparison to the solution pertaining to an initial condition with $\omega(y_s, 0) \neq 0$. We note as well that, for an antisymmetric initial condition, ω_i becomes a symmetric function in $[-1, 1]$. In this section, for sake of brevity, we presented the evolution of the imaginary part of the solution. The real part of the vorticity, ω_r, shows analogous features. The only significant difference is that, for the profile $f(y) = y^3 - 0.49y$, ω_r is symmetric in $[-1, 1]$ for even $\omega(y, 0)$ and antisymmetric for odd $\omega(y, 0)$.

To gain a better insight on the mechanism responsible for the present growth we studied the evolution of the perturbation streamfunction. Results are given in figures 7 and 8, where the evolution of the real part of the streamfunction is presented. They clearly show its global exponential decay. For the profile $y^3 - 0.49y$ the decay is not phase dependent. The imaginary part of the streamfunction shows an analogous behaviour and therefore we decided not to present the relative figures.

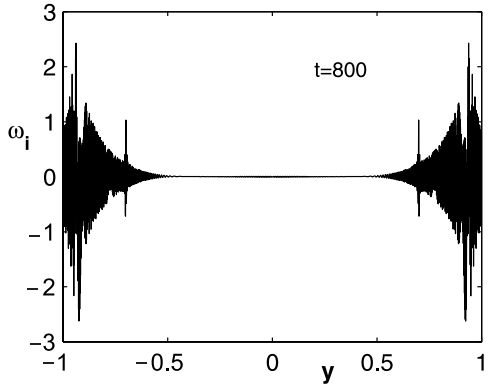

Figure 6. Imaginary part of the disturbance at $t = 800$ for $f(y) = y^3 - 0.49y$ and $\omega(y, 0) = \sin(y)$.

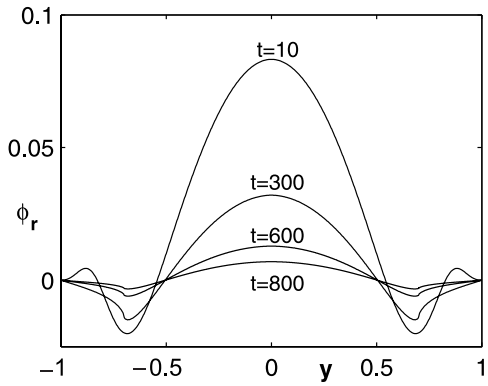

Figure 7. Global evolution of the real part of the streamfunction for $f(y) = y^3 - 0.49y$ and $\omega(y, 0) = \cos(y)$.

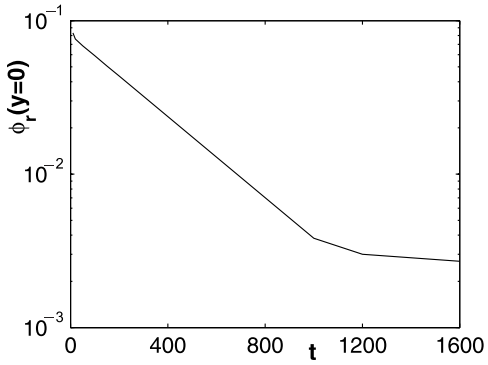

Figure 8. Evolution of the real part of the streamfunction at $y = 0$ for $f(y) = y^3 - 0.49y$ and $\omega(y, 0) = \cos(y)$.

The picture which arises from these results is consistent with the mechanism found in [1], where decay of the disturbance streamfunction occurred in combination with the formation of a vorticity bump at the resonant layer y_c given by the relation $kf(y_c) = \mathrm{Re}(c_L)$, where c_L is the complex frequency (Landau pole) governing the streamfunction evolution.

To ascertain whether the decay of the streamfunction is due to a Landau pole, we carried out simulations relative to initial conditions of the type $\omega(y, 0) = \cos^p(y)$ up to $p = 5$. For all the cases the decay rate for the streamfunction turned out to be $\mathrm{Im}(c_L) \sim 0.003\,04$. This shows that the decay rate is independent on the details of the initial vorticity disturbance. This is a feature which characterizes Landau poles, whose value depends only on the equilibrium profile.

A direct numerical computation of the Landau pole will be performed in section 4. The results will confirm what found above.

3. Eigenspectrum analysis

To interpret the results obtained in the previous section it is beneficial to perform an eigenmode analysis of equation (12). We will rely on the methods described in [1, 13], where the Rayleigh equation in cylindrical coordinates was studied. Assuming solutions of the type $\omega = \xi(y)\,\mathrm{e}^{\mathrm{i}ct}$, equation (12) becomes

$$c\xi(y) = kf(y)\xi - kf''(y)\int_{-1}^{1} G(y, \bar{y})\xi(\bar{y})\,\mathrm{d}\bar{y} \equiv B[\xi]. \tag{13}$$

The spectrum of the operator B has a discrete and a continuous component. The continuous component is given by the purely real eigenfrequencies in the range

$$\min_{y\in[-1,1]}(kf(y)) < c < \max_{y\in[-1,1]}(kf(y)). \tag{14}$$

We recall here that, in the usual understanding, eigenfunctions relative to discrete eigenvalues are spatially smooth, while those relative to continuum eigenvalues are singular.

Eigenmode analysis was carried out numerically. We followed [13] and discretized the spatial coordinate y into N points in $[-1, 1]$. This converts the operator B into an $N \times N$ matrix. We computed eigenvalues and eigenvectors of both B and its transpose B^T. We denote ξ as an eigenvector of B and c as its eigenvalue. ξ_T and c_T denote eigenvector and eigenvalue of B^T. Eigenvectors are normalized to unity with respect to the Euclidean norm $\left(\int_{-1}^{1} \xi^*\xi\,\mathrm{d}y = 1\right)$. The set of eigenvalues for B and B^T is the same, but the eigenvectors are not equal. They, however, enjoy the property

$$\langle \xi, \xi_T \rangle = 0 \qquad \text{if} \qquad c \neq c_T^*, \tag{15}$$

where

$$\langle g, h \rangle = \sum_{i=1}^{N} g^*(y_i)h(y_i). \tag{16}$$

We assumed that the vorticity perturbation can be approximated by the expansion

$$\omega(y_i, t) = \sum_{j=1}^{N} A_j \xi_j(y_i)\,\mathrm{e}^{\mathrm{i}c_j t}, \tag{17}$$

where ξ_j and c_j represent the jth eigenvector and eigenvalue of B.

This assumption is arbitrary since there is no proof that eigenvectors of B form a complete system. Furthermore we stress that expansion (17) is by no means a spectral decomposition of ω, but just a numerical approximation. However, we will see that it leads to results in close agreement with those obtained in the previous section. The coefficients A_j can be calculated from

$$A_j = \frac{\langle \xi_{T,j}, \omega(y, 0) \rangle}{\langle \xi_{T,j}, \xi_j \rangle}, \tag{18}$$

where $\xi_{T,j}$ is the eigenvector of B^T corresponding to the eigenvalue c_j^*.

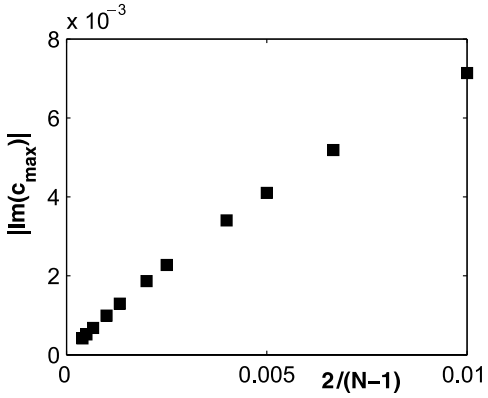

Figure 9. Dependence of the growth rate (Im[c]) of the most unstable eigenvalue on the grid-point spacing $2/(N-1)$.

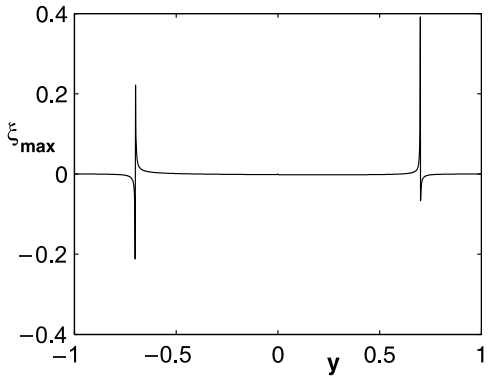

Figure 10. Vorticity eigenmode corresponding to the eigenvalue with largest growth rate ($N = 2001$).

We computed the eigenvalues of B for various values of N. No eigenvalue presents a dominant negative imaginary part, moreover the imaginary parts of the eigenvalues decrease with increasing N. For the profile $f(y) = y^3 - 0.49y$ the most unstable eigenvalue is purely imaginary. In figure 9, we give the dependence of its absolute value on the grid-point spacing $2/(N-1)$. This leads to the conclusion that in the limits of our analysis either all the eigenvalues are spurious [13] or, if a truly unstable eigenvalue is present, its growth rate is so small that it turns out to be not relevant for the time scales here treated. A confirmation of this is given in figure 10 where is presented the imaginary part of the eigenfunction relative to the most unstable eigenvalue, which shows singular behaviour at $y = \pm 0.7$. All complex eigenfunctions have a singular shape. This is at odds with the common understanding of discrete eigenmodes, which are characterized by smoothness.

In order to gain a precise understanding of the eigenmode structure we plotted in figure 11 the same eigenfunction of figure 10 but with a smaller range of ξ-values. It can be noted, together with the spikes at $y = \pm 0.7$, the presence of an extended bulk component. As shown in [1] bulk components of continuum modes can be important in the formation of a quasimode, a vorticity perturbation which behaves in the early dynamics like an exponentially damped wave [4].

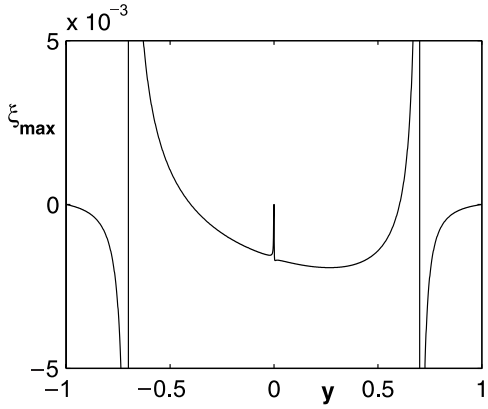

Figure 11. Close-up of the vorticity eigenmode corresponding to the eigenvalue with largest growth rate ($N = 2001$).

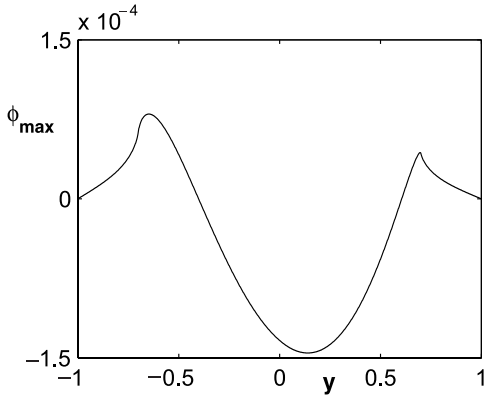

Figure 12. Streamfunction eigenmode corresponding to the eigenvalue with largest growth rate ($N = 2001$).

In figure 12 we plot the streamfunction corresponding to the vorticity eigenmode of figure 10. As shown in the figure the dominant component of $\phi_{\max}$ is determined by the bulk component of $\xi_{\max}$. The real part of the eigenmode relative to the most unstable eigenvalue shows features very similar to those given in figures 10–12 and therefore we do not present it.

Figure 13 shows equation (17) for the profile $f(y) = y^3 - 0.49y$ and the initial condition $\omega(y, 0) = \cos(y)$ at $t = 800$. The results are in agreement with those of the previous section.

A deeper understanding of how the growth occurs is obtained by plotting the absolute value of the coefficients A_j of the eigenfunctions as functions of the real part of the relative eigenvalue. As evident from figure 14, the A_j become dominant near $\mathrm{Re}(c_j) = 0$. This confirms the resonant growth obtained from the initial-value problem where the peaks of the solution occurred at $f(y_p) = 0$. For a profile of the type $f(y) = a + y^3 - by$ we found that the A_j become singular around $\mathrm{Re}(c_j) = kf(y_s)$ (where y_s is defined by $f''(y_s) = 0$), which is the phase corresponding to the points y_p such as $f(y_p) = f(y_s)$.

Suppression of growth occurring for initial vorticity perturbations vanishing at the inflection point can be understood by plotting the relative $(\mathrm{Re}(c_j), |A_j|)$ graph. Figure 15 shows that the value of the coefficients near $\mathrm{Re}(c_j) = 0$ is drastically reduced and this decrease

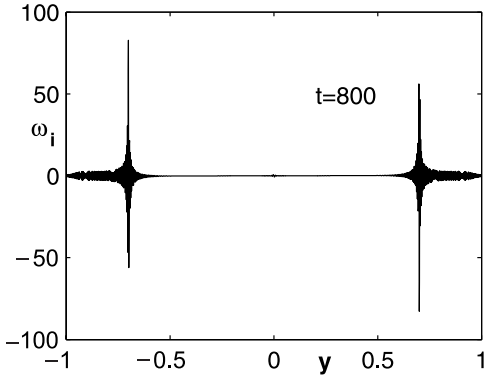

Figure 13. Eigenmode expansion (17) evaluated at $t = 800$ ($N = 2001$).

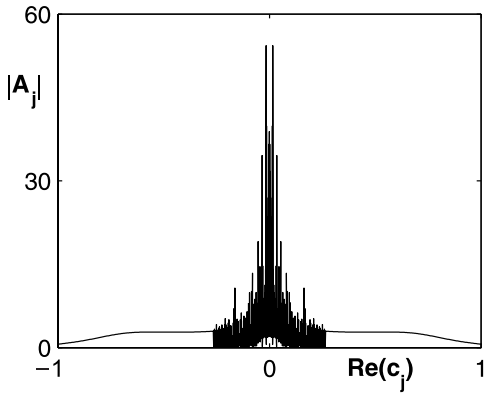

Figure 14. Absolute value of the expansion coefficients A_j for the initial condition $\omega(y, 0) = \cos y$ ($N = 2001$).

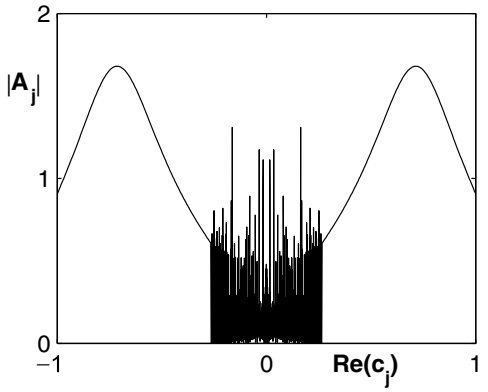

Figure 15. Absolute value of the expansion coefficients A_j for the initial condition $\omega(y, 0) = \sin y$ ($N = 2001$).

causes the lack of growth. We note that the rapid fluctuations of $|A_j|$ in figures 14 and 15 are due to the degeneracy of the continuum modes which occurs in non-monotonic flows.

We computed the eigenspectra of the profiles under study for different values of b. What we have numerically found is that for $b < 0.85$ fast exponential instabilities do not occur for any value of the wave number k. For $b > 0.85$ and opportune values of k powerful Kelvin–Helmholtz like instabilities take place. These results are confirmed by the numerical integration of the initial-value problem.

The picture arising is that a Landau pole c_L leads to a saturated growth of an initial perturbation with coefficients $|A_j|$ peaked around $\mathrm{Re}(c_L)$. The saturation value for the vorticity perturbation can be found heuristically by substituting

$$\phi(y,t) = A(y)\,\mathrm{e}^{\mathrm{i}c_L t} \tag{19}$$

in equation (9). $A(y)$ is a function which can be extrapolated from the numerical results. We obtain

$$[\partial_t - \mathrm{i}kf(y)]\omega = \mathrm{i}kf''(y)A(y)\,\mathrm{e}^{\mathrm{i}c_L t}. \tag{20}$$

Integration of the above equation leads to the expression

$$\omega = \mathrm{i}kf''(y)A(y)\,\mathrm{e}^{\mathrm{i}kf(y)t}\int_0^t \mathrm{e}^{\mathrm{i}c_L s}\,\mathrm{e}^{-\mathrm{i}kf(y)s}\,\mathrm{d}s. \tag{21}$$

For $f(y) = y^3 - 0.49y$ we have a Landau frequency $\mathrm{Re}(c_L) = kf(y_s) = 0$ and a Landau decay rate for the streamfunction $\gamma_L = \mathrm{Im}(c_L) \sim 0.003\,04$. Considering that $f(y_p) = 0$ in y_p we have

$$\omega(y_p,t) = \mathrm{i}kf''(y_p)A(y_p)\frac{1-\mathrm{e}^{-\gamma_L t}}{\gamma_L}. \tag{22}$$

Substituting into the above expression $k = 2$ and the numerical values relative to $y_p = -0.7$ ($f''(-0.7) = -4.2$ and $\mathrm{Re}(A(-0.7)) = -0.033$) we obtain for the imaginary part of the vorticity perturbation the following saturation value:

$$\omega_i(-0.7, t = \infty) \sim 92, \tag{23}$$

which is in good agreement with the one found in the numerical simulations ($\sim$90).

The ratio $\frac{1-\mathrm{e}^{-\gamma_L t}}{\gamma_L}$ on the right-hand side of (22) suggests the definition of a saturation time $\tau_{\mathrm{sat}} = \frac{4.6}{\gamma_L}$, which is the time required to have $\mathrm{e}^{-\gamma_L t} \approx \frac{1}{100}$. τ_{sat} will be used in the following section to discuss the dependence of the Landau pole c_L on the wave number k.

To conclude this section we emphasize that the validity of the numerical scheme here presented was tested with the same model profiles ($\sin \beta y$, Poiseuille, etc) used in the previous section, reproducing the eigenspectra given in the existing literature. Expansion (17) for the model profiles gives results fully consistent with those computed by the numerical integration scheme of the previous section.

For the profile under study ($f(y) = y^3 - 0.49y$) the range of the continuous spectrum ($[-1.02, 1.02]$) was correctly computed.

4. Numerical calculation of the Landau pole

In this section, we will confirm the results obtained previously, which suggested the existence of a Landau pole with imaginary part $\gamma_L \approx 0.003\,04$. This will be done by numerically computing the Landau pole using a technique developed in [14] and based on the analytical treatment of [4]. A good review of the material is given in the appendix of [1].

Our treatment will slightly differ with the one in [14] in two respects. First, the geometry here is flat while there was cylindrical. Second, the profile here is non-monotonic while there was monotonic.

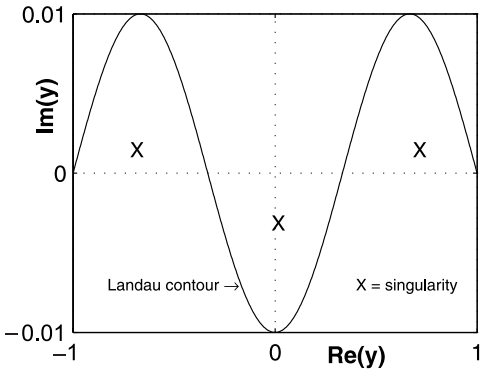

Figure 16. Example of Landau bypass contour in the y-plane for the non-monotonic profile $f(y) = y^3 - 0.49y$ and wave number $k = 2$.

Following closely the above-mentioned references, we start from equation (9). Substituting $\phi(y) = \tilde{\phi}(y)\,\mathrm{e}^{\mathrm{i}ct}$ and dividing through by $c - kf(y)$ we obtain

$$\left[\partial_y^2 - k^2 + \frac{kf''(y)}{c - kf(y)}\right]\tilde{\phi}(y, c) = 0. \tag{24}$$

This equation presents a branch cut in the complex c-plane for

$$\min_{y\in[-1,1]}(kf(y)) < c < \max_{y\in[-1,1]}(kf(y)). \tag{25}$$

The idea exposed in [4, 14] is to analytically continue $\tilde{\phi}(y, c)$ in the c-plane by deforming the branch line in the semiplane $\mathrm{Im}(c) > 0$. If the new branch line, defined by $kf(\mathrm{Re}(y) + \mathrm{i}\,\mathrm{Im}(y)) = c$, bends sufficiently above the real axis, a Landau pole may be uncovered. In [4, 14] the profile $f(y)$ was monotonic, therefore the anti-image of c_L/k in the complex y-plane, was a single point. In our case, being $f(y)$ non-monotonic c_L/k can have up to three anti-images. This fact suggests that some additional care must be taken in choosing the Landau contour in the y-plane. In our case, for example, we are looking for a Landau pole $c_L \approx \mathrm{i}\,0.003\,04$. Anti-images of c_L through $f(y)$ are

$$y_{1,2} \approx \pm 0.7 + \mathrm{i}\,0.001\,55, \qquad y_3 \approx -\mathrm{i}\,0.0031. \tag{26}$$

This means that the Landau contour in the y-plane has to pass below y_3 and above y_1 and y_2. In other words the uncovering of c_L in the c-plane creates three singularities in the y-plane, which are pushed through the real axis in directions that depend on the value of $f'(y)$ at the crossing points [15]. For the profile $f(y) = y^3 - 0.49y$, $f'(\mathrm{Re}(y_1)) > 0$ and $f'(\mathrm{Re}(y_2)) > 0$ imply that the Landau contour has to pass above y_1 and y_2. Instead since $f'(\mathrm{Re}(y_3)) < 0$ the bypass contour passes below y_3.

According to the above considerations, we have chosen a sinusoidal contour of the type shown in figure 16 with analytical dependence

$$y(s) = s + \mathrm{i}A\cos\tfrac{3}{2}\pi s, \qquad -1 \leqslant s \leqslant 1, \tag{27}$$

A is a constant used to adjust the bending of the contour $y(s)$. Integrated along $y(s)$ equation (24) becomes

$$\left[\frac{\mathrm{d}}{\mathrm{d}s}\frac{1}{y'(s)}\frac{\mathrm{d}}{\mathrm{d}s} - y'(s)k^2 + \frac{ky'(s)f''(y(s))}{c - kf(y(s))}\right]\tilde{\phi}(s, c) = 0. \tag{28}$$

We need three boundary conditions to solve the above eigenproblem, which are easily determined considering that

$$\tilde{\phi}(y, c) \to \sinh(k(1 + y)) \qquad \text{as} \quad y \to -1. \tag{29}$$

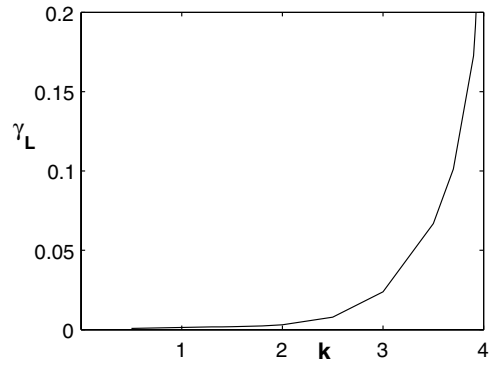

Figure 17. Dependence of the Landau pole on the wave number k.

In fact the above limit implies

$$\tilde{\phi}(-1+\varepsilon, c) = \sinh[k(1+y(-1+\varepsilon))], \tag{30}$$

$$\frac{\mathrm{d}}{\mathrm{d}s}\tilde{\phi}(-1+\varepsilon, c) = ky'(-1+\varepsilon)\cosh[k(1+y(-1+\varepsilon))], \tag{31}$$

where ε is a positive number $\ll 1$. The third condition is simply

$$\tilde{\phi}(1, c) = 0. \tag{32}$$

Equation (28) with the boundary conditions (30)–(32) can be solved numerically with various methods such as finite element or shooting to determine the value of the Landau pole, if existent. For the case $k = 2$ and $f(y) = y^3 - 0.49y$, we obtained for c_L a value in close agreement with the one determined in the previous two sections

$$c_L = \mathrm{i}0.003\,0423. \tag{33}$$

We computed as well the dependence of the value of the Landau pole on the wave number k. We have found that c_L is proportional to k as shown in figure 17. We noted that at $k \approx 3.93$ and above (we investigated up to $k = 4$) two Landau poles are uncovered instead of a single one. This pair of poles are one the opposite complex conjugate of the other—if c_L is one then $-c_L^*$ is the other. This fact is not shown in figure 17.

We conclude this section with a note on the relation between the saturation value reached by the vorticity at y_p ($f(y_p) = 0$) and the value of the Landau pole.

Referring to equation (22), we can see that, assuming $A(y_p)$ as almost constant, the ratio $\frac{k}{\gamma_L}$ gives the size of the maximum growth achievable. For the profile $f(y) = y^3 - 0.49y$ we have found that $\frac{k}{\gamma_L}$ is maximum around $k = 1.5$. Therefore we expect to achieve maximum vorticity growth for this value of k. This is indeed what we have obtained from the numerical integration of the initial-value problem and from the solution of the eigenspectrum analysis, both predicting a saturation value for the imaginary part of the vorticity of $\omega_i(y_p, \infty) \approx 110$.

It is interesting to see how enstrophy and energy of the modes evolve with time. We defined enstrophy and energy of the kth wave number component, respectively as

$$W = \int_{-1}^{1} \omega^*(y,t)\omega(y,t)\,\mathrm{d}y, \qquad E = \int_{-1}^{1} \mathbf{v}^*(y,t)\cdot\mathbf{v}(y,t)\,\mathrm{d}y. \tag{34}$$

Evolution of these quantities is shown in figures 18 and 19, for $k = 1, k = 1.5$ and $k = 2$. For k below 1 the enstrophy saturates to values lower than that shown in figure 18 (for

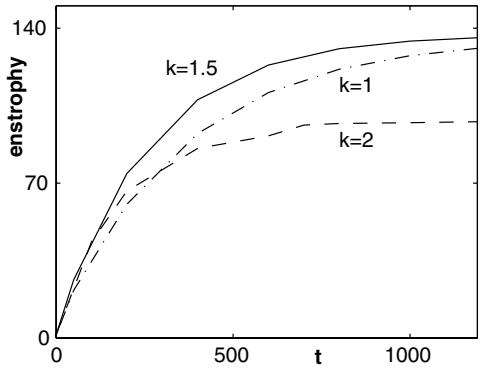

Figure 18. Evolution of the enstrophy for different k for the initial condition $\omega(y, 0) = \cos y$.

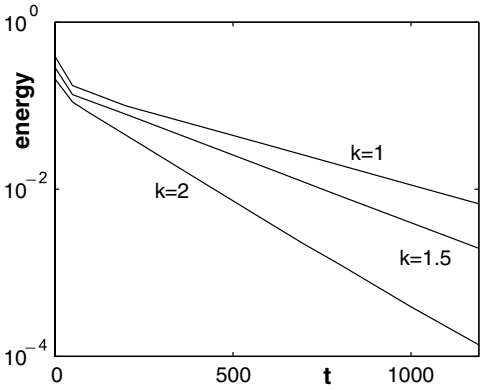

Figure 19. Evolution of the energy for different k for the initial condition $\omega(y, 0) = \cos y$.

$k = 0.5$, $W_{\text{sat}} \approx 65$). For k above 2 the saturation value progressively diminishes and, above $k = 3$, τ_{sat} is so short that the enstrophy turns out to be almost constant at very low values (for $k = 3.9$, $W_{\text{sat}} \approx 2$).

The evolution of the energy (figure 19) shows, as expected, an exponential decrease with a decay rate given by $2\gamma_L$.

5. Summary

We have presented a linear resonant mechanism which leads to the growth of two-dimensional inviscid vorticity in non-monotonic shear flows of the type $f(y) = a + y^3 - by$. The vorticity perturbation grows to a saturation value in the vicinity of the points y_p where the flow velocity $f(y)$ is in resonance with its value at the inflection point y_s. The growth mechanism closely resembles the one found in [1], where the decay of the primary component of the vorticity perturbation was accompanied by its moderate growth at a resonant layer determined by the real part of a Landau pole of the system. In the present case, the growth saturates to values of order 10^2 of the peak of the initial vorticity perturbation. Another peculiar feature of the present growth is represented by its critical dependence on the value of the initial condition at the inflection point y_s. Namely, the vanishing of the initial disturbance at y_s essentially inhibits the growth mechanism. This is due to the fact that the expansion coefficients of initial

perturbations peaked around the inflection point tend to diverge at frequencies $\mathrm{Re}(c) \sim 0$ (figure 14), while the coefficients of initial disturbances which vanish at the inflection point stay close to moderate values (figure 15). This feature is analogous to the behaviour found in [16]. There the local algebraic growth, occurring in the Rayleigh equation in the presence of shear flows endowed with a stationary point of high order, was shown to depend critically on the value of the initial disturbance at the stationary point itself.

A comment is due regarding the results of the eigenvalue analysis. In section 3 we showed that, in the limit of our analysis, either all the complex eigenvalues are spurious or, if a truly unstable eigenvalue was present, it would have a growth rate so small to give a negligible contribution in the time scales relevant for the present study. Spurious eigenvalues are characterized by the vanishing of their imaginary parts as N, the number of points by which we approximate the interval $[-1, 1]$, tends to infinity. In other words they would belong to the continuous spectrum. This speculation seems to be confirmed by the fact that the associated eigenmodes are singular. In fact, as well known, eigenfunctions corresponding to continuous eigenvalues are singular.

The non-normal dynamics of optimal perturbations has been shown recently to play a central role in the onset of turbulence in various fluid systems: viscous channel flows [17, 18], inviscid and viscous unbounded constant shear flows [19], atmospheric vortices [20], the Lamb–Oseen vortex [21], etc. The kinetic energy of such perturbations can increase by thousands of times before asymptotically decaying to zero with time. In our case, instead, the vorticity growth in the resonance layers is accompanied by the global exponential decay of streamfunction and velocity components, therefore as shown in section 4 no energy growth for perturbations pertains. On the other side there could be similarities between the growth mechanism discussed in our study and the growth of optimal perturbations. We refer in particular to the strong dependence of the vorticity growth on the initial perturbation shape. Another possible point of contact could be the fact that as it occurs for optimal perturbations, exponential decay leads ultimately to transient growth of the perturbation. However, the equations and the profiles here studied present differences with those investigated in the references above; this fact renders a close comparison with optimal perturbation dynamics quite difficult. Therefore from our results we cannot draw any definitive conclusion about the relationship between Landau pole induced saturated growth of the vorticity perturbation and the transient energy amplification of optimal perturbations.

Due to the analogy existing between 2D inviscid incompressible fluids and 2D low-density electron beams [4] the present vorticity growth mechanism could be checked experimentally either with neutral fluids or with electron plasmas. As seen above the component of the initial vorticity disturbance that drives the growth of ω in the resonance layers is situated at the inflection points y_s of the mean flow where $\frac{\mathrm{d}^2}{\mathrm{d}y^2} f(y_s) = \frac{\mathrm{d}}{\mathrm{d}y}\Omega_0(y_s) = 0$. However, as shown in [1], the potential flow associated with an external impulse applied at the channel boundary ($y = \pm 1$) excites vorticity perturbations only in points for which holds $\frac{\mathrm{d}}{\mathrm{d}y}\Omega_0 \neq 0$. Therefore generation of initial vorticity disturbances by the application of external impulses at the boundary it is not a suitable experimental procedure for the verification of the vorticity growth mechanism here presented. The creation of a favourable initial vorticity disturbance could be achieved, for example, by the application of an impulse directly at the inflection point of the equilibrium profile. Many other, more efficient, procedures can be devised.

At last we note that, in spite of the fact that the type of equilibrium profiles studied satisfy the Rayleigh–Fjørtoft necessary condition for instability, no fast exponential instability was found to occur for any wave number k for $b < 0.85$. For $b > 0.85$ and opportune values of k global exponential growth takes place.

References

[1] Schecter D A, Dubin D H E, Cass A C, Driscoll C F, Lansky I M and O'Neill T M 2000 *Phys. Fluids* **12** 2397
[2] Smith R A and Rosenbluth M N 1990 *Phys. Rev. Lett.* **64** 649
[3] Ingersoll A P 1990 *Science* **248** 308
[4] Briggs R J, Daugherty J D and Levy R H 1970 *Phys. Fluids* **13** 421
[5] Bassom A P and Gilbert A D 1998 *J. Fluid Mech.* **371** 109
[6] Corngold N R 1995 *Phys. Plasmas* **2** 620
[7] Rayleigh J W S 1880 *Proc. Lond. Math. Soc.* **9** 57
[8] Fjørtoft R 1950 *Geofys. Publ.* **17** 1
[9] Case K M 1960 *Phys. Fluids* **3** 143
[10] Dikii L A 1960 *Sov. Phys. Dokl.* **135** 1179
[11] Rosencrans S I and Sattinger D H 1966 *J. Math. Phys.* **45** 289
[12] Drazin P G and Reid W H 1984 *Hydrodynamic Stability* (Cambridge: Cambridge University Press) p 151
[13] Schecter D A 1999 *PhD Dissertation* University of California, San Diego
[14] Spencer R L and Rasband S N 1997 *Phys. Plasmas* **4** 53
[15] Schmid P J and Henningson D S 2001 *Stability and Transition in Shear Flows* (New York: Springer) p 44
[16] Volponi F 2005 *J. Phys. A: Math. Gen.* **38** 4293
[17] Farrell B F 1988 *Phys. Fluids* **31** 2093
[18] Butler K M and Farrell B F 1992 *Phys. Fluids* A **4** 1637
[19] Farrell B F and Ioannou P J 1993 *Phys. Fluids* A **5** 1390
[20] Nolan D S and Farrell B F 1999 *J. Atmos. Sci.* **56** 1282
[21] Antkowiak A and Brancher P 2004 *Phys. Fluids* **16** L1